Electronic Supporting Information

Electrospun Protein Nanofibers with Nanoscale Morphological Control for Dopamine Biosensing

Katarzyna Kolodzinska,[1*] Sylwia Baluta,[1] Adrian Cernescu,[2] Magdalena Wojtas,[1] Maciej Lipok,[1] Joanna Olesiak-Bańska,[1] Joanna Cabaj[1] and Lech Sznitko[1*]

[1]Faculty of Chemistry, Wroclaw University of Science and Technology, Wybrzeze Wyspianskiego 27, 50-370 Wroclaw, Poland

[2]Neaspec—Attocube Systems AG, Eglfinger Weg 2, Haar, 85540, Munich, Germany

E-mail addresses: katarzyna.kolodzinska@pwr.edu.pl, lech.sznitko@pwr.edu.pl

Content

1. Experimental Section

1.1 Materials

Materials: Polyethylene oxide (M_w 900000 g· mol^{-1}, Sigma-Aldrich), Bovine serum albumin (BSA, 98% purity, Angene), Laccase (EC 1.10.3.2, from *Trametes versicolor*, ≥10 U mg^{-1}), and dopamine hydrochloride (DA) were obtained from Sigma-Aldrich Co. (Merck). Ascorbic acid (AA), tyrosine (Tyr), uric acid (UA), and urea were also purchased from the same supplier. Citric acid, sulfuric acid, sodium hydroxide, sodium phosphate, potassium phosphate, TRIS, hydrochloric acid, sodium acetate, acetic acid, sodium chloride, potassium chloride, and glutaraldehyde (GA) were sourced from POCH (Avantor, Performance Materials, Poland). All chemicals were of analytical grade and used without further purification. Buffers were prepared according to standard protocols.

1.2 Solution preparation

PEO (M_w 900000 g· mol^{-1}, Sigma-Aldrich) was dissolved in a solvent mixture of distilled water and dimethylformamide (DMF, analytical standard) in a 7:3 (v/v) ratio at concentrations of 1% and 1.5% (w/w). Solutions were stirred and heated on a hot plate at 75°C for 4h. After cooling to room temperature, BSA was added to the earlier prepared PEO solutions without further purification to obtain a protein concentration of 8.9% or 8.4% in the final solution.

1.3 Electrospinning

Electrospinning BSA/PEO solutions with different protein and polymer concentrations was performed in a horizontal setup (Spinbox by Bioinicia Fluidnatek apparatus, Spain) at a temperature range of 24-28°C and a humidity range of 36-40%. The distance between the nozzle and the collector was 15 cm, and a voltage of 13 kV was applied to the nozzle. For BSA/PEO fiber fabrication, a stainless steel needle with a 22-gauge inner diameter (0.41 mm) and an outer diameter of 0.71 mm was used. The flow rate of the electrospun solution was 0.4 ml/h.

1.4 Transmission electron microscopy

Transmission electron microscopy (TEM) imaging of electrospun fibers was performed using a Talos F200i transmission electron microscope (Thermo Fisher Scientific) with an accelerating voltage of 200 kV. For TEM imaging, sample preparation involved directly depositing electrospun fibers onto TEM grids coated with carbon film. Depending on the analyzed samples, the fibers were crosslinked and functionalized in the same manner as those

produced on platinum electrodes (*Methods section: Dopamine detection: Electrochemical analysis and biosensor construction*). The average fiber and bead diameters were calculated using ImageJ software from 100 measurements.

1.5 Bulk FTIR spectral measurements

The bulk chemistry of BSA, PEO, and electrospun materials was analyzed using Attenuated Total Reflectance-Fourier Transform Infrared (ATR-FTIR) spectroscopy (Jasco FT/IR-6700). Measurements were conducted on BSA and PEO in their commercial crystalline forms without further purification. Electrospun materials were used directly for measurements, without additional crosslinking steps.

1.6 Nano-FTIR spectral measurements

Nano-infrared imaging and spectroscopy were performed using a commercial scattering-type near-field microscope (IR-neaSCOPE+s, attocube.com) with tunable and broadband mid-IR lasers. A quantum cascade laser (MIRcat, Daylight Solutions) provided monochromatic IR focused on a metallized AFM tip (tapping mode) to detect scattered near-field signals. A pseudoheterodyne Michelson interferometer extracted optical amplitude and phase while minimizing background, enabling simultaneous topography, nanoIR absorption, and nanoIR reflectivity imaging at ~20 nm resolution. Broadband nano-FTIR spectroscopy used a difference-frequency generated mid-IR source (Toptica Photonics), with interferometric detection via an asymmetric Michelson interferometer for acquisition of nanoscale localized nanoFTIR spectra.

1.7 Analysis of Nano-FTIR spectral measurements

Nano-FTIR spectra between 1600-1720 cm^{-1} for selected locations for each structure were averaged and normalized. Using Origin Pro 2023b software for the spectra, applied peak deconvolution. Then, the spectra were analyzed based on literature data [1–3] concerning FTIR spectra for secondary protein structures in the examined region. The fitting analysis of the spectra was required to converge and meet a Chi-squared tolerance criterion of 1×10^{-6}.

1.8 Determination of molecular ordering with polarization-sensitive two-photon fluorescence microscopy

Polarization-sensitive two-photon fluorescence microscopy technique enables the examination of the relationship between two-photon fluorescence intensity and the linear polarization direction of the excitation beam, along with the analysis of the polarization of the emitted fluorescence. The assumptions and procedure were described in detail in the

publication. [4] Two-photon excited luminescence imaging was performed with a custom-built system consisting of the excitation light source: fs Ti:Sapphire laser (~100 fs, 80 MHz, Chameleon, Coherent Inc.) combined with an inverted microscope. To set the polarization of the excitation light, the laser beam was passed through a half-wave plate mounted on a rotation stage. The samples were mounted on an XYZ piezoelectric scanning stage (Piezojena, TRITOR 102) and scanned to obtain images. The polarized laser beam was reflected by a dichroic mirror and focused on the sample using a high-numerical-aperture objective (Nikon Plan Apo Oil Immersion 100x/1.4 NA). The backward emitted signal was collected by the same objective and split by a polarizing beam-splitter into two orthogonally polarized beams (Ix and Iy) to be detected by two photon-counting avalanche photodiodes (IDQ id100). The two-photon excited emission spectra were measured with a spectrograph (Shamrock 303i Andor). For the electrospun fibers, an autofluorescence was excited at 810 nm.

1.9 Fluorescent confocal microscopy with Fluorescence Lifetime Imaging

Fluorescent confocal microscopy with fluorescence lifetime imaging was performed using a TCS SP8 or Stellaris 8 (Leica) confocal laser scanning microscope. Samples of electrospun fibers were prepared on glass slides and covered with coverslips. One-photon excited autofluorescence emission measurements were conducted for 405 nm excitation. However, fluorescence lifetime measurements and imaging were performed at an excitation wavelength of 415 nm due to equipment limitations. Image acquisition and fluorescence lifetimes calculations were carried out using Leica Application Suite X (LasX).

1.10 Dopamine detection: Electrochemical analysis and biosensor construction

All electrochemical experiments were performed using an Autolab PGSTAT 128N potentiostat/galvanostat controlled by NOVA software, employing a three-electrode cell setup. The working electrode was a platinum electrode (PtE) with a 3 mm diameter (BASi, MF-2013 model), either modified or unmodified. A silver/silver chloride electrode (saturated KCl) served as the reference electrode, while a platinum wire functioned as the counter electrode.

To construct the biosensors, platinum electrodes (3 mm diameter, BASi, MF-2013) were used as the working electrode, with nanofibers composed of BSA:PEO electrospun directly onto their surface and cross-linked in 5% GA vapors for 3h to fabricate a non-soluble in water matrix. Two immobilization strategies for laccase were employed: physical adsorption onto

the nanofiber matrix followed by cross-linking with 5% GA for 4 hours, and the second approach, where laccase was incorporated directly within the nanofibers during fabrication.

The electrospinning process was carried out as described in the *Methods Section: Electrospinning* for a solution with a 90:10 BSA-to-PEO ratio after 4 hours of mixing to obtain bead-free fibers (C type). For the second approach, the laccase was added at a final concentration of 0.6 mg/ml (Sigma-Aldrich) 30 minutes before electrospinning, and then the process was carried out as described. Modified electrodes after cross-linking in 5% GA were subsequently washed twice with 0.1 M phosphate buffer (pH 7.0), followed by a 45-minute wash with 0.1 M Tris-HCl buffer (pH 7.2) to remove unbound proteins.

To assess enzyme activity in the presence of dopamine (in 0.1 PBS buffer at pH 7.0), cyclic voltammetry (CV) was employed in the potential range -0.1 – 0.6 V, with a scan rate 50 mV s^{-1} *vs* Ag/AgCl electrode. Although laccase exhibits optimal activity at slightly acidic pH values around 5, we utilized a phosphate-buffered saline (PBS) buffer at pH 7 to mimic physiological conditions relevant to real-world applications. [5] The modified PtE/BSA:PEO NFs/Lac electrodes, prepared as described, were stored at 8 °C when not in use to maintain their stability. The CV measurements were conducted over a potential range of -0.1 to 0.6 V at a scan rate of 50 mV s^{-1} for three cycles under ambient conditions in an 8-mL cell. For a more sensitive analysis, differential pulse voltammetry (DPV) was employed to evaluate key performance parameters of the biosensors, including linearity, selectivity, and detection limit, within a potential range of 0 to 0.4 V. DA standard solutions were prepared by dissolving DA in 0.1 M PBS buffer at pH 7.0, reflecting the conditions used for laccase immobilization, and were analyzed across concentrations from 2.5 to 200 µM. The resulting current responses were found to be proportional to the corresponding dopamine concentrations.

To investigate potential interference, a DA solution (100 µM) was spiked with AA, UA, urine, and Tyr, each at a concentration of 100 µM. The impact of these substances was evaluated using DPV under conditions identical to those employed for dopamine detection. To assess stability, the biosensors were subjected to DPV in the presence of DA two weeks after fabrication.

2. Influence of solvent, composition, and pH-dependent stability on electrospun BSA:PEO nanofibers

Based on literature reports on the electrospinning of protein–polymer systems (BSA with PEO), [6] it has been shown that increasing the protein content (from 5 to 20 wt%) at a constant PEO concentration (3 wt%) significantly increases the average fiber diameter. Relying on this knowledge, in the present work, we aimed to achieve the lowest possible PEO content relative to BSA while maintaining fiber diameters below 500 nm. This is crucial for electrochemical sensing applications, as a higher surface-to-volume ratio enhances analyte–sensor interactions and consequently improves sensitivity. Moreover, a higher protein content enhances structural stability and reduces nonspecific binding, thereby facilitating the efficient and durable immobilization of the catalytic enzyme (laccase) responsible for dopamine oxidation.

Moreover, according to the results [6], PEO concentration plays a more critical role in solution viscosity than the absolute BSA amount. Therefore, the optimization initially focused on the appropriate ratio of the PEO content to BSA. Starting from 0.5% PEO (BSA to PEO ratio 95:5) resulted in electrospraying rather than fiber formation. When the PEO concentration was increased to 1% (BSA to PEO ratio 90:10), the viscosity became sufficient to enable stable fiber formation after BSA addition, leading to reproducible, thicker materials (Figure S1 A-B).

Among the tested organic solvents intended to reduce surface tension and partially unfold the BSA structure to improve the stability of electrospinning BSA with added PEO, three solvents were evaluated: DMF, DMSO, and acetonitrile. Each of them has a much lower surface tension than water (77.66 mN/m), with the following values for DMF, DMSO, and acetonitrile: 35.83, 42.70, and 28.49 mN/m. [7,8] The solvents were mixed with water at a 3:7 volume ratio (organic solvent:water). The PEO concentration in the solution was 1.5% w/w, after which BSA was added to obtain a final BSA:PEO mass ratio of 85:15. Electrospun fibers were produced from each solution, and their microscopic images based on BSA autofluorescence measurements are compared in Figure S1 C-E.

Based on these observations, it can be concluded that the addition of acetonitrile resulted in the formation of beads with irregular shapes, while the fibers produced with DMSO exhibited nonhomogeneous structures consisting of fibers and fibers with beads, with inconsistent diameters and varying fiber thicknesses. Only the use of DMF resulted in a reproducible fiber structure. Due to the importance of controlling the material morphology, particularly the

uniform distribution of protein within the samples, further studies were carried out using water and DMF in a 7:3 ratio.

To ensure the suitability of the nanofibers for biosensing applications within the physiologically relevant pH range (5–7), their stability under varying pH conditions was examined. After crosslinking in glutaraldehyde vapor, the membranes were immersed in PBS at pH 5 or 7 to assess potential morphological changes. Based on the measured fiber diameters (Figure S1 F-G), no significant differences were observed, indicating that pH variations are not expected to affect the suitability of the fibers for sensing applications.

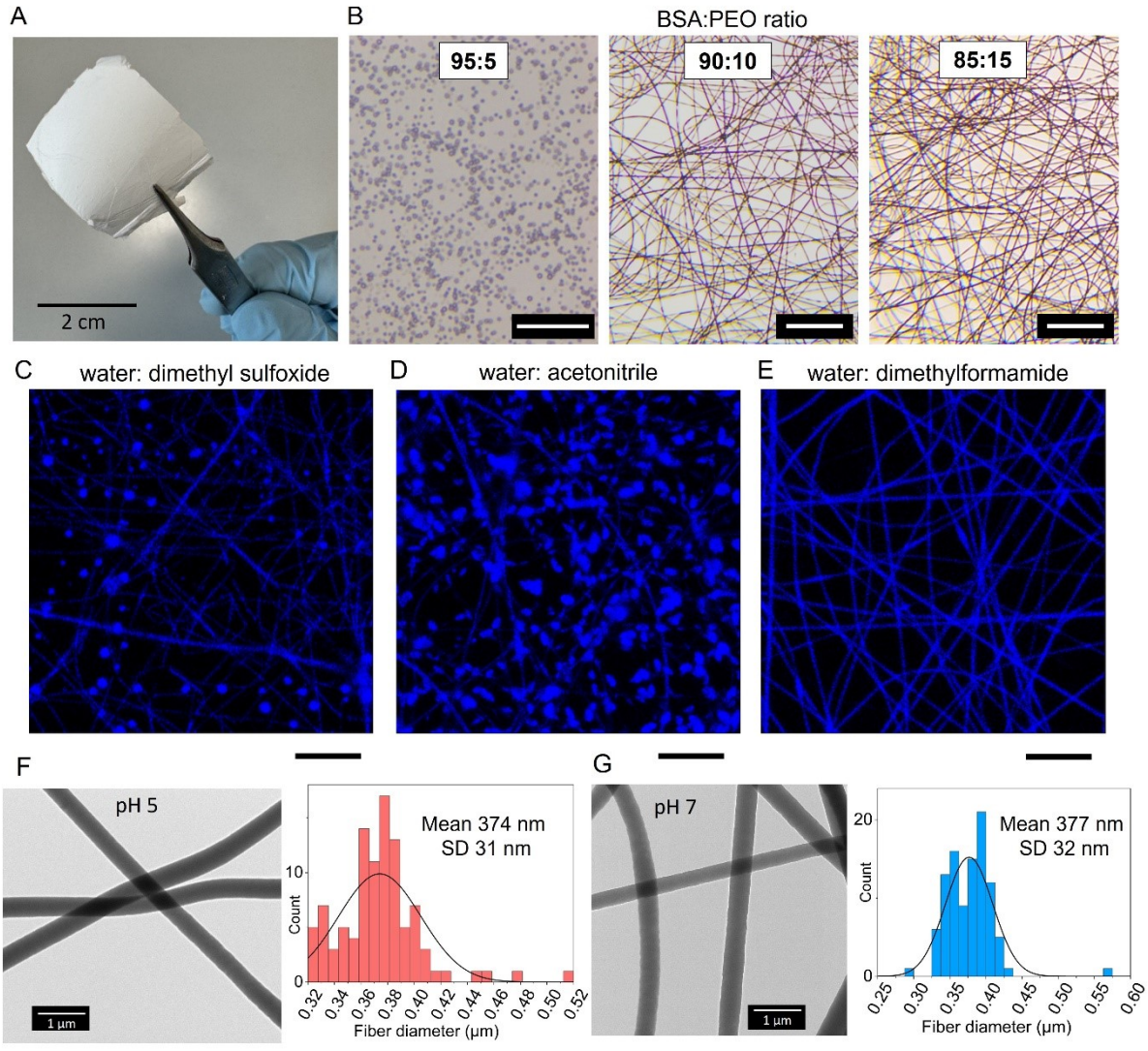

Figure S1. Thick electrospun fabric obtained for the 90:10 BSA:PEO ratio (free-standing mat) (A)**.** Morphology of electrospun fibers produced using different BSA:PEO ratios — 95:5 (scale bar: 25 µm), 90:10 (scale bar: 5 µm), and 85:15 (scale bar: 5 µm) (B). Morphology of electrospun fibers obtained from solutions prepared with different solvent mixtures: water:DMSO (C), water:acetonitrile (D), and water:dimethylformamide (E); scale bars for C–E:

10 µm. Electrospun fibers after treatment at pH 5 with corresponding fiber diameter distribution (F) and after treatment at pH 7 with corresponding fiber diameter distribution (G).

3. FTIR-ATR spectroscopy for electrospun fibers

To check the presence and proportion of BSA and PEO in the electrospun fibers, ATR-FTIR measurements were conducted for samples of fibers with BSA:PEO ratios of 90:10 and 85:15. This technique allows the examination of the sample by providing an averaged result for a larger volume of the material. The crystalline form of the BSA and PEO served as references for subsequent measurements. The ATR spectrum (Figure S2) acquired for electrospun fibers with higher PEO content shows more intensive signals of -C-O-C- absorption around 1100 cm^{-1} as a result of a combination of ether group and methylene group stretching, CO/CH_2 rocking/stretching around 840 cm^{-1}, and C-H stretching around 2880 cm^{-1}. [9,10] The mentioned peak positions of PEO are also in good agreement with PEO crystal form measurements and literature. [9,10]

From the FTIR-ATR spectrum of the BSA in crystalline form and electrospun BSA-based fibers, the two most characteristic absorption bands can be identified: the Amide I and Amide II bands (Figure S2). The Amide I band (1600–1700 cm^{-1}), attributed to C=O stretching vibrations, [11] remains unchanged between crystalline BSA and electrospun BSA-based fibers with varying BSA:PEO ratios and morphologies, with a peak at 1650 cm^{-1}. However, the amide II band (1480–1580 cm^{-1}), associated with C-N stretching and N-H bending, [12] exhibits a slight peak shift between 1517 cm^{-1} for crystalline BSA and 1538 cm^{-1} for electrospun fibers. Moreover, the intensity of Amide II absorption is lower in electrospun fibers compared to the pure BSA in crystalline form. This may be linked to molecular arrangement and intermolecular interactions, particularly hydrogen bonding in different secondary structures. [12,13] Furthermore, BSA is more organized in its crystalline state than in the form of electrospun fibers, forming a more rigid structure that results in a more pronounced and distinct vibrational mode for the Amide II band. [13] Regarding different BSA:PEO ratios, no shift in the absorption peaks for Amide II was observed; however, the intensity was slightly higher for the 90:10 ratio compared to the 85:15 ratio.

Moreover, in Figure S2, the FTIR-ATR spectra for electrospun materials and crystalline BSA show strong absorption between 2870-2920 cm^{-1} due to C-H stretching vibration of CH_3 and CH_2 and 3100- 3600 cm^{-1} connected to the stretch vibrational mode of N-H and O-H groups. The intensity of these bands was the highest for the protein in its crystalline form and gradually decreased with a lower protein proportion in the material, confirming the protein-to-PEO ratio in the fabricated materials.

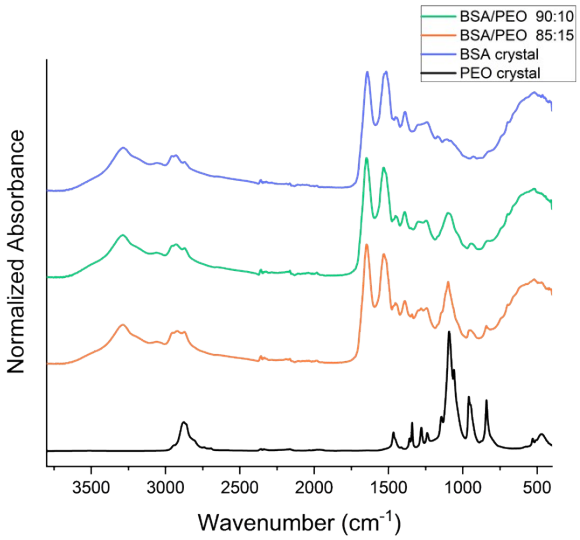

Figure S2. FTIR-ATR spectra for electrospun fibers in ratio 90:10 (green line) and ratio 85:15 (orange line), BSA in crystalline form (blue line), and PEO in crystalline form (black line).

4. AFM profile across a tiny fiber

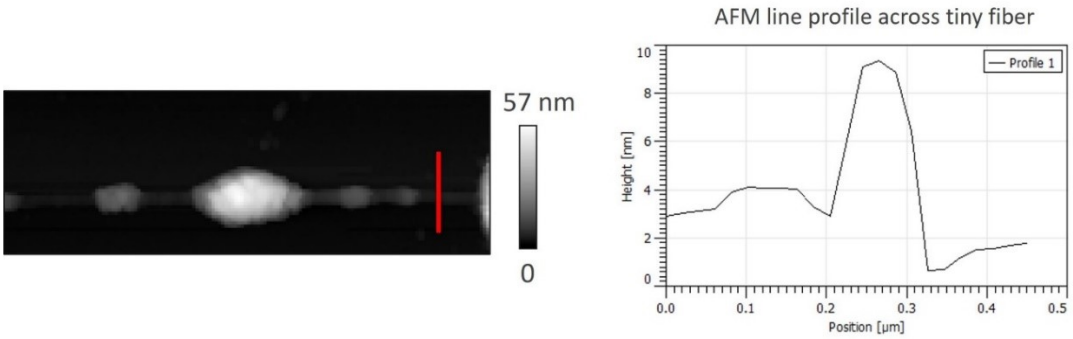

Figure S3. AFM profile across a tiny fiber – measurement at the location marked in red.

5. Nano-FTIR spectrum for electrospun bead-less fibers

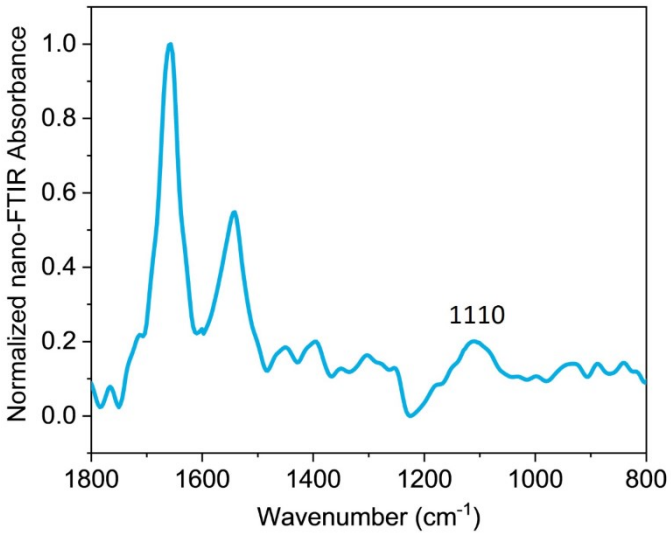

Figure S4. Nano-FTIR for electrospun bead-less fibers observed IR with a wide peak at around 1110 cm $^{-1}$ corresponding to amorphous PEO form.

6. One-photon and two-photon excited autofluorescence of BSA-based fibers spectra and fluorescent lifetimes

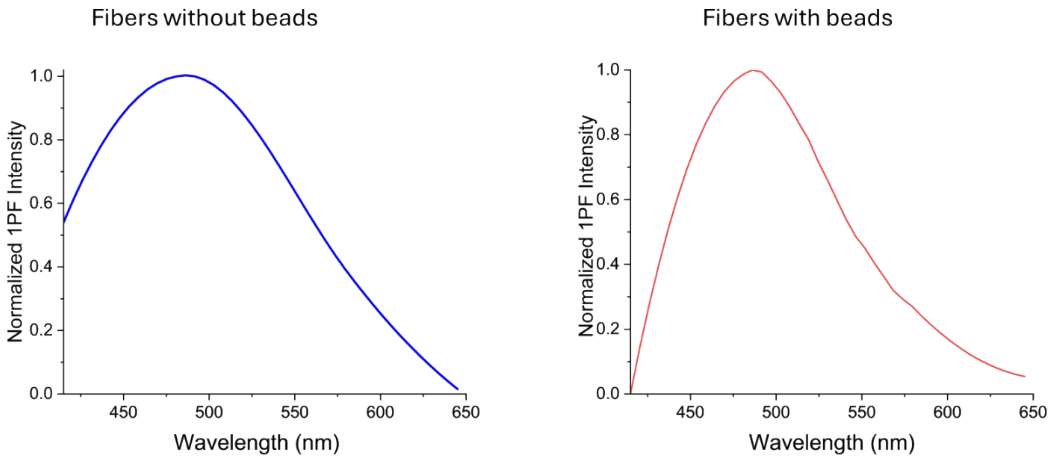

Figure S5. One-photon excited autofluorescence of BSA-based fibers spectra. Excitation at 405 nm.

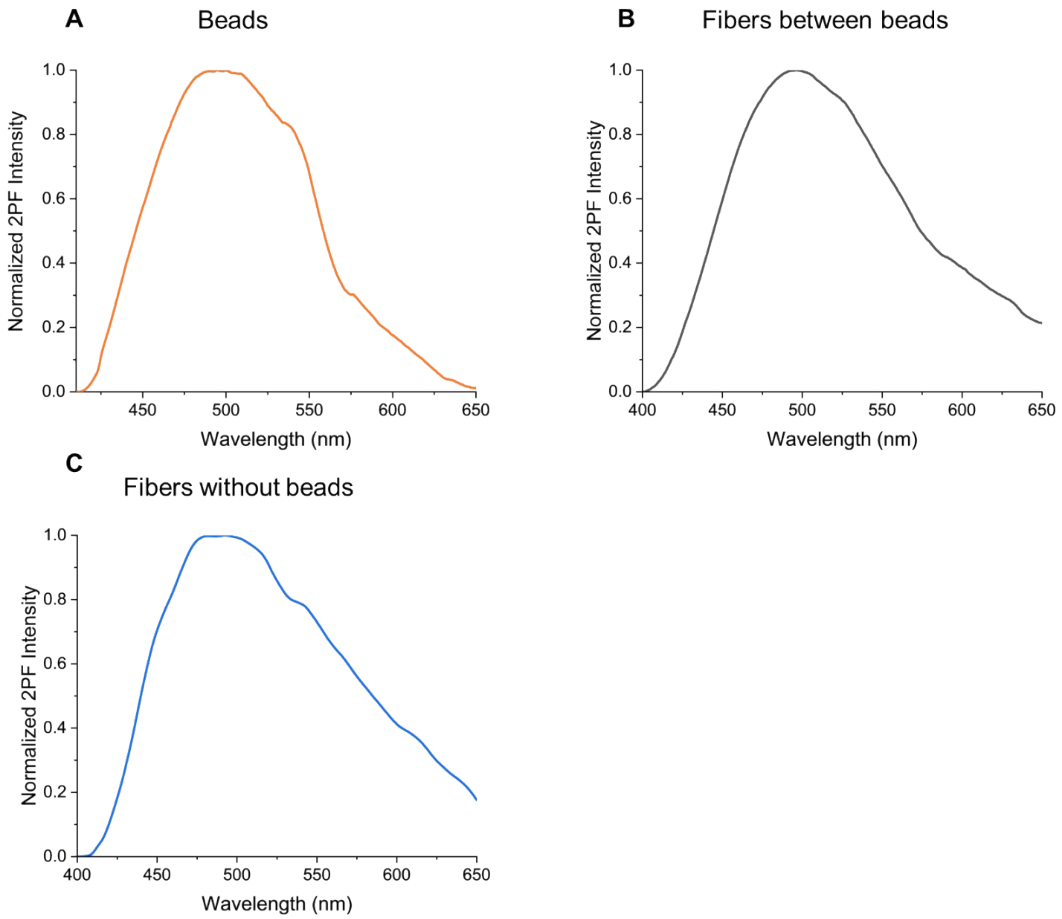

Figure S6. Two-photon excited autofluorescence spectra of: beads in beaded fibers structure (A), fibers between beads (B) in beaded fibers structure, and fibers in fibrous structure without beads (C). Excitation at 810 nm for all measurements.

Table S1. Fluorescence lifetimes for beads and fibers of BSA-based electrospun structures. Excitation at 415 nm. The fluorescence decay for all structures was fitted with a monoexponential model.

Electrospun structure	Fluorescence lifetime (ns)	χ^2
A-Type beads	2.37 ± 0.25	1.263
B-Type beads	2.36 ± 0.16	1.161
Fiber between beads	2.18 ± 0.27	1.028
Bead-free fibers	2.20 ± 0.22	0.974

7. A schematic representation of the Ψ, ΔΨ, and Φ angles within the XY plane

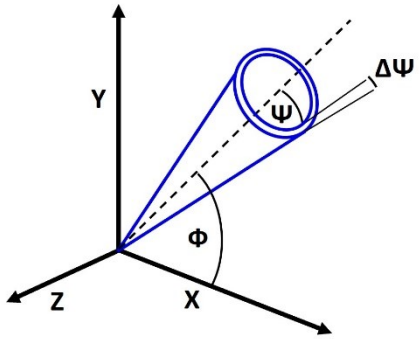

Figure S7. A schematic representation of the Ψ, ΔΨ, and Φ angles within the XY plane.

8. The intensity of the two-photon excited autofluorescence distribution for: electrospun bead-free fibers and beaded fibers.

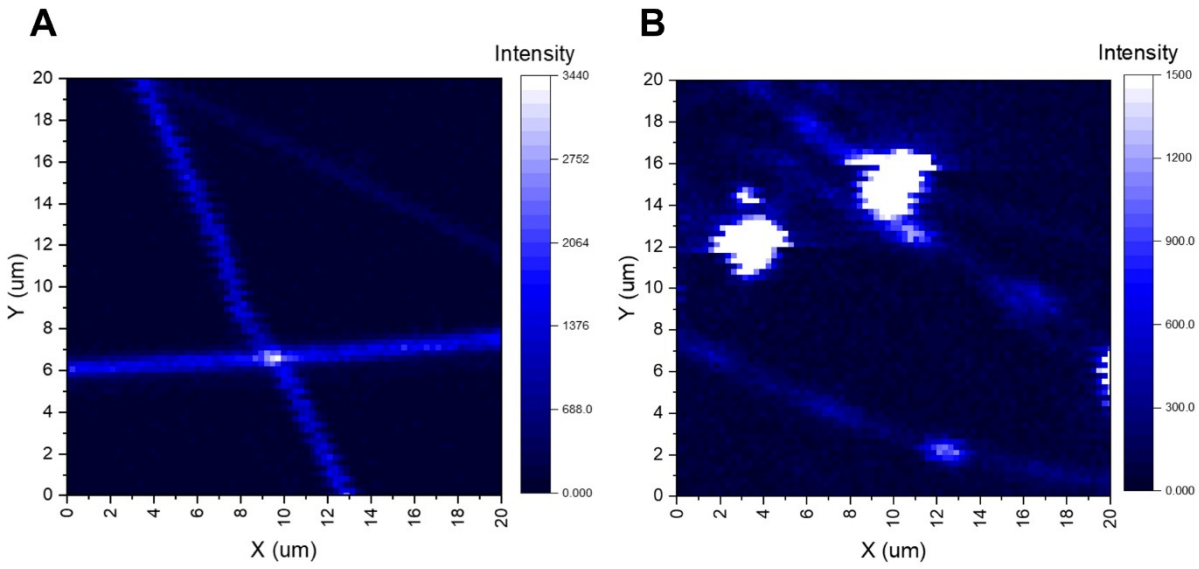

Figure S8. The intensity of the two-photon excited green autofluorescence distribution for: electrospun bead-free fibers (A) and beaded fibers (B).

9. Sensing mechanism of dopamine

The catalytic mechanism of laccase toward dopamine (DA) oxidation is well established and has been thoroughly described in the literature, [14–17] including in the previous works of the co-author, Sylwia Baluta. [18–20] In this work, laccase was employed as a model enzyme to demonstrate the potential of the fabricated nanofibers (NFs), which constitute the main focus of this study, for future applications, i.e., in biosensing.

Laccase, a widely studied and cost-effective enzyme, is particularly suitable for biosensor applications due to its high stability, enzymatic activity, and ability to catalyze the oxidation of phenolic compounds, including dopamine, a neurotransmitter with remarkable redox properties critical for electrochemical detection. [21] Dopamine's unique electrochemical behavior allows it to serve as a model substrate in biosensing studies, where its oxidation can be precisely monitored.

To check the whole redox process and present the enzymatic activity of the laccase immobilized on the modified electrode, the cyclic voltammetry (CV) method was performed. As shown in Figures 7 E and B in the main manuscript, the biosensor's responses and whole redox process were examined in the presence and absence of dopamine by applying the CV method. The buffer alone (black line) did not exhibit any redox signals, whereas dopamine (violet/blue line) displayed a distinct oxidation peak at the potential value 0.22 V, which corresponds to the DA oxidation region.[22]. Also, a very small reduction peak from the laccase can be seen near 0.6 V. Laccase, a member of the oxidoreductase family, is a protein capable of facilitating direct electron transfer (DET).[23] It contains in its active center four copper atoms: T1, T2, and two T3, distinguished by their spectroscopic characteristics. Notably, the T1 copper center in laccase can be reduced at higher potential values (around and higher than 0.6 V) [24] by compounds such as DA [25–27].

In both voltammograms, it is evident that DA is oxidized, accompanied by a region characteristic of the reduction from the active center of laccase (T1 cluster). The system with laccase immobilized onto the surface of the nanofibers exhibited a wider oxidation signal, while the system with laccase immobilized inside the nanofibers showed a sharper oxidation peak. This difference could be attributed to the fact that the internal immobilization may facilitate more efficient electron transfer and better-defined redox processes, leading to enhanced sensitivity and analytical performance. In CV, a sharper oxidation signal is generally preferred over a wider peak for analytical purposes. Sharper peaks indicate better-defined redox processes and higher sensitivity, which are crucial for accurately determining the electrochemical behavior of the analyte.[28] It could also be attributed to the fact that when laccase is immobilized inside the NFs, it creates a confined microenvironment that enhances electron transfer efficiency and stabilizes the enzyme, leading to sharper oxidation signals during CV. Conversely, laccase immobilized on the surface of the NFs may experience less

direct interaction with the electrode and a broader diffusion layer, resulting in wider oxidation signals. What is more, received CV-scans confirmed that the observed electrochemical signals are exclusively due to dopamine, unaffected by the buffer composition.

10. Linear relationship between the current and dopamine, where laccase has been immobilized onto the nanofibers' surface and inside the nanofibers

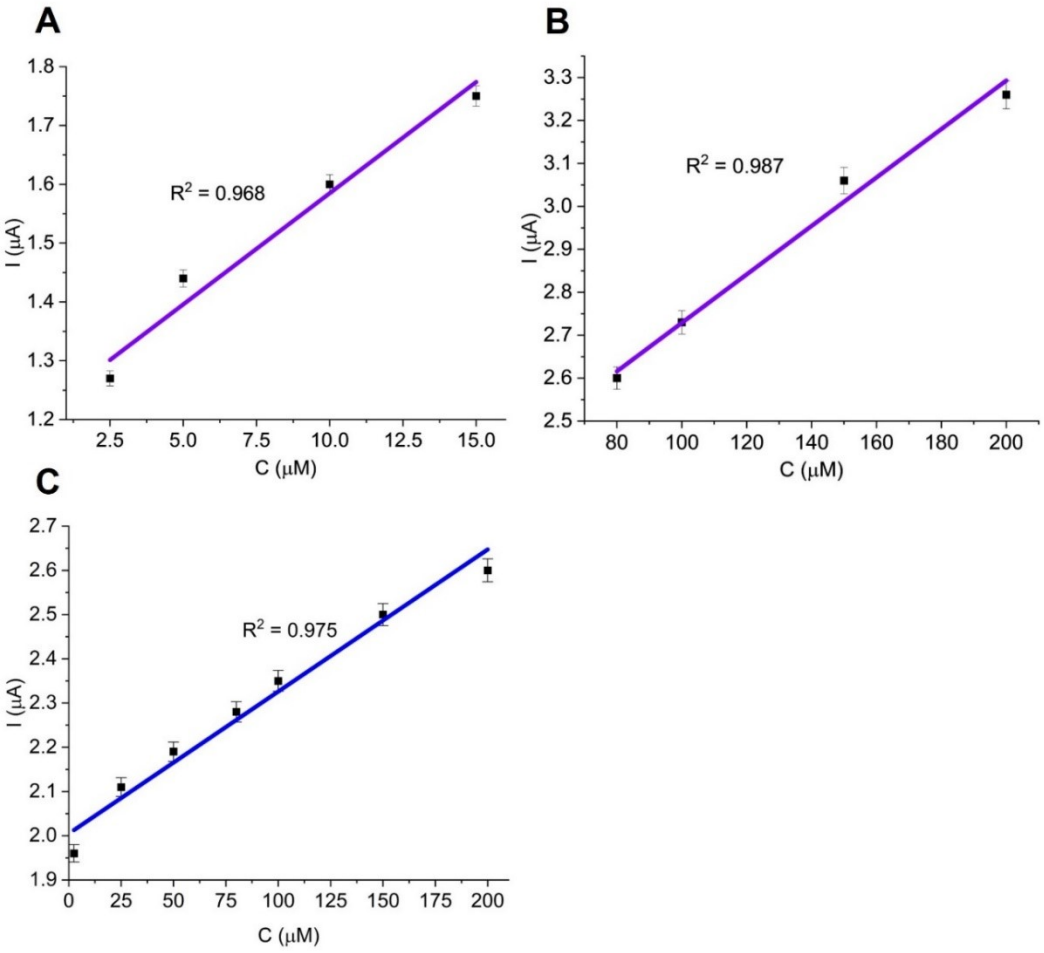

Figure S9. Linear relationship between the current and dopamine, where laccase has been immobilized onto the nanofibers' surface for: the lower concentration range (2.5-15 μM) (A) and the: higher concentration range (80-200 μM) (B). Linear relationship between the current and dopamine, where laccase has been immobilized inside the NFs. Potential range 0-0.4 V via Ag/AgCl (C).

References

1 A. Dong, P. Huang and W. S. Caughey, Biochemistry 1990; **29** (13), 3303-3308.

2 H. Yang, S. Yang, J. Kong, A. Dong and S. Yu, *Nat Protoc*, 2015, **10**, 382–396.

3 H. A. Alhazmi, M. S. Alam, M. Albratty, A. Najmi, A. A. Abdulhaq, R. Hassani, W. Ahsan and A. N. Qramish, *J Chem*, DOI:10.1155/2023/2581653.

4 M. Lipok, P. Obstarczyk and J. Olesiak-Bańska, *Journal of Visualized Experiments*, 2023, 199. DOI:10.3791/65670.

5 S. Baluta, K. I. Duerme, W. K. M. Perera, A. Szyszka, P. Jamróz and J. Cabaj, *Colloids Surf A Physicochem Eng Asp*, 2025, **718**, 136873 DOI:10.1016/j.colsurfa.2025.136873.

6 R. Díaz-Puertas, E. Rodríguez-Cañas, M. J. Lozoya-Agulló, P. V. Badía-Hernández, F. J. Álvarez-Martínez, A. Falcó and R. Mallavia, *Int J Biol Macromol*, 2024, **280**, 136019. DOI:10.1016/j.ijbiomac.2024.136019.

7 W. J. Cheong and P. W. Carr, *J Liq Chromatogr*, 1987, **10**, 561–581.

8 H. Kahl, T. Wadewitz and J. Winkelmann, *J Chem Eng Data*, 2003, **48**, 580–586.

9 I. Pucić and T. Jurkin, *Radiation Physics and Chemistry*, 2012, **81**, 1426–1429.

10 C. Bergeron, E. Perrier, A. Potier and G. Delmas, *Int J Spectrosc*, 2012, **2012**, 1–13, 432046.

11 C. Guo, X. Guo, W. Chu, N. Jiang and H. Li, *Chinese Chemical Letters*, 2019, **30**, 1302–1306.

12 A. S. Chatterley, P. Laity, C. Holland, T. Weidner, S. Woutersen and G. Giubertoni, *Molecules*,2022, **27** (19). DOI:10.3390/molecules27196275.

13 L. P. Deflores, Z. Ganim, R. A. Nicodemus and A. Tokmakoff, *J Am Chem Soc*, 2009, **131**, 3385–3391.

14 R. Wu, S. Yu, S. Chen, Y. Dang, S. H. Wen, J. Tang, Y. Zhou and J. J. Zhu, *Anal Chim Acta*, 2022, **9**, 1229, 340365. DOI:10.1016/j.aca.2022.340365.

15 R. K. Shervedani and A. Amini, *Bioelectrochemistry*, 2012, **84**, 25–31.

16 J. H. Coelho, A. P. P. Eisele, C. F. Valezi, G. J. Mattos, J. G. Schirmann, R. F. H. Dekker, A. M. Barbosa-Dekker and E. R. Sartori, *Talanta*, 2019, **204**, 475–483.

17 L. Xiang, Y. Lin, P. Yu, L. Su and L. Mao, *Electrochim Acta*, 2007, **52**, 4144–4152.

18 S. Baluta, D. Zając, A. Szyszka, K. Malecha and J. Cabaj, *Sensors,* 2020, **20**, 2, 423. DOI:10.3390/s20020423.

19 S. Baluta, K. Malecha, D. Zając, J. Sołoducho and J. Cabaj, *Sens Actuators B Chem*, 2017, **252**, 803–812.

20 S. Baluta, A. Lesiak and J. Cabaj, *Electroanalysis*, 2018, **30**, 1773–1782.

21 M. M. Rodríguez-Delgado, G. S. Alemán-Nava, J. M. Rodríguez-Delgado, G. Dieck-Assad, S. O. Martínez-Chapa, D. Barceló and R. Parra, *Elsevier B.V.*, 2015, preprint, DOI: 10.1016/j.trac.2015.05.008.

22 H. Xu, L. Wang, J. Luo, Y. Song, J. Liu, S. Zhang and X. Cai, *Sensors,* 2015, **15**, 1008–1021.

23 R. S. Freire, C. A. Pessoa, L. D. Mello and L. T. Kubota, *Direct Electron Transfer: An Approach for Electrochemical Biosensors with Higher Selectivity and Sensitivity*, 2003, 14.

24 C. Adam, P. Scodeller, M. Grattieri, M. Villalba and E. J. Calvo, *Bioelectrochemistry*, 2016, **109**, 101–107.

25 I. V Berezin, S. D. Varfolomeev and M. V Lomonosov, in *Enzyme Engineering: Volume 5*, eds. H. H. Weetall and G. P. Royer, Springer US, Boston, 1980, 95–100.

26 C.-W. Lee, H. B. Gray, F. C. Anson and B. G. Malmström, *J Electroanal Chem Interfacial Electrochem*, 1984, **172**, 289–300.

27 F. Xu, W. Shin, S. H. Brown, J. A. Wahleithner, U. M. Sundaram and E. I. Solomon, *Biochimica et Biophysica Acta (BBA) - Protein Structure and Molecular Enzymology*, 1996, **1292**, 303–311.

28 N. Elgrishi, K. J. Rountree, B. D. McCarthy, E. S. Rountree, T. T. Eisenhart and J. L. Dempsey, *J Chem Educ*, 2018, **95**, 197–206.